sustainability

MDPI

Article

Seasonal Differences in Water-Use Sources of *Impatiens hainanensis* (Balsaminaceae), a Limestone-Endemic Plant Based on "Fissure-Soil" Habitat Function

Weixia Huang [1,2], Yunfang Zhong [1], Xiqiang Song [1,3,*], Cuili Zhang [1], Mingxun Ren [1] and Yanjun Du [1,3]

[1] Key Laboratory of Genetics and Germplasm Innovation of Tropical Special Forest Trees and Ornamental Plants, Ministry of Education, Hainan University, Haikou 570228, China; Huangweixia1210@163.com (W.H.); kitty@hainanu.edu.cn (Y.Z.); 15008092531@163.com (C.Z.); renmx@hainanu.edu.cn (M.R.); 993801@hainanu.edu.cn (Y.D.)
[2] College of Life and Pharmaceutical Sciences, Hainan University, Haikou 570228, China
[3] College of Forestry, Hainan University, Haikou 570228, China
* Correspondence: songstrong@hainanu.edu.cn

Abstract: The southwestern mountains of Hainan Island are the southernmost region with tropical karst landform in China. The frequent alternation of dry and wet seasons leads to the loss of the mineral nutrients of limestone, creating karst fissure habitats. Plants living in karst fissure habitats for long periods of time have developed local adaptation mechanisms correspondingly. In the paper, hydrogen–oxygen stable isotope technology was applied to determine the water-use sources of *Impatiens hainanensis* in the dry and wet seasons, hoping to expound the adaptation mechanism of *I. hainanensis* in karst fissure habitats to the moisture dynamics in the wet and dry seasons. In the wet season (May to October, 2018), the air humidity is relatively high in the *I. hainanensis* habitat; in the dry season (November 2018 to April 2019), there is a degree of evaporation. In the wet season, fine-root biomass increases with soil depths, while coarse-root biomass decreases with soil depths; in the dry season, fine-root biomass is lower and coarse-root biomass is higher compared with the wet season. It was found that the average rainfall reached 1523 mm and the main water-use sources were shallow (0–5 cm) and middle (5–10 cm) soil water, epikarst water, and shallow karst fissure water during the wet season; the average rainfall reached 528 mm, and the deep (10–15 cm) soil water and shallow karst fissure water were the main water-use sources during the dry season. Fog water has a partial complementary effect in the dry season. The differences in the distribution of root biomass and each source of water in the wet and dry seasons of *I. hainanensis* also reflect the different water-use strategies of *I. hainanensis* in the wet and dry seasons. In both dry and wet seasons, *I. hainanensis* formed a water-use pattern dominated by soil water and shallow fissure water (0–15 cm) under the influence of the "fissure-soil-plant" system in the karst region.

Keywords: *Impatiens hainanensis*; karst; shallow fissures; hydrogen–oxygen stabilized isotopes; water utilization

check for updates

Citation: Huang, W.; Zhong, Y.; Song, X.; Zhang, C.; Ren, M.; Du, Y. Seasonal Differences in Water-Use Sources of *Impatiens hainanensis* (Balsaminaceae), a Limestone-Endemic Plant Based on "Fissure-Soil" Habitat Function. *Sustainability* **2021**, *13*, 8721. https://doi.org/10.3390/su13168721

Academic Editor: Bernhard Huchzermeyer

Received: 3 July 2021
Accepted: 30 July 2021
Published: 4 August 2021

Publisher's Note: MDPI stays neutral with regard to jurisdictional claims in published maps and institutional affiliations.

Copyright: © 2021 by the authors. Licensee MDPI, Basel, Switzerland. This article is an open access article distributed under the terms and conditions of the Creative Commons Attribution (CC BY) license (https://creativecommons.org/licenses/by/4.0/).

1. Introduction

The environment governs the geographical distribution, growth, and developmental status of plants, but the environment is influenced by plants at all times [1]. In the soil–plant–atmosphere continuum, plant water is influenced by environmental physical factors such as soil, air moisture limitation, and the regulation of organisms themselves [2]. Water is the most important limiting factor for ecosystem processes and functions in deserts and ecologically fragile areas [3], and it plays a critical role in plant growth and development, survival, and distribution [4]. The intensity and frequency of precipitation determine the survival, composition, structure, and functional assemblage of plant species in ecosystems [5]. In the context of global climate change, changes in precipitation patterns, in

particular, have important implications for individual plant water sources, water-use strategies, and vegetation distribution, as well as ecosystem water balance [6]. The response of ecosystems to climate change is influenced to some extent by plant water-use patterns [7], and different life forms have different sources of water use, resulting in differences in their response to climate change [8,9]. Plants growing in karst desert areas have been affected by arid ecological environments for a long time and have not only evolved morphologically and structurally with characteristics adapted to the arid environment [10] but also strong heterogeneity in physiological characteristics [11]. Stable isotope techniques are used to study water bodies such as atmospheric precipitation, soil water, groundwater, and plant water as a whole system, to quantitatively elucidate the processes and mechanisms of water transport, transformation, and distribution in each water, and to reflect the ecology of soil–plant–atmosphere at the individual, community, and ecosystem scales [12,13].

Shallow karst fissures are parts of the karst critical zone that are in direct contact with the soil. In karst areas, these shallow fissures are the main places where relatively deep soils are stored [14]. When surface soils are scarce, shallow karst fissures are not only the main conduit for subsurface leakage but are also an important soil storage space in karst areas [15–17]. Soil filling of fissures changes the characteristics of fissure water transport, which in turn affects water processes in karst areas [18,19]. The filling of soil by shallow karst fissures creates a unique "rock-fissure-soil" microhabitat (or shallow karst fissure habitat) [20,21], which provides a relatively well-coordinated water and fertilizer stand for plant growth.

The filtering influence of karst habitats on islands is characterized by seasonal and localized spatial heterogeneity. Rainwater run-offs leach limestone mineral nutrients, which results in calcium-rich alkaline soils and the formation of "heterogeneous environmental sieves" such as stone gaps and crevices. Local microhabitats have increased the amount of natural shade intensity and reduced plant water transpiration [22,23]. The "heterogeneous environmental sieves" are relatively more habitat-friendly, and the ecological stress in the karst landscape is weakened. The highly heterogeneous and diverse shallow karst fissure habitats reduce the stress-limiting effects of the karst "heterogeneous environmental sieve" and maintain the relative stability of microhabitat species [24,25], creating a favorable environment for plant survival. The local adaptation processes of endemic plants to shallow karst fissure habitats in tropical karst locations [19], in particular, the ecological response of karst-specific plants to heterogeneous environmental sieves, suggest karst-specific plants have adapted to living in rocky fissure habitats and dealing with water stressors. Have karst-specific plants that grow in shallow rocky fissure habitats for long periods of time developed unique adaptation mechanisms to deal with water stressors here?

Hainan Island is located in the southernmost part of China and is the largest tropical island in China [26]. Located at the northern edge of the tropics, Hainan Island is a typical tropical monsoon climate zone with a maximum interval of 47.6 ± 16.1 d between typhoons; dry and wet seasons are obvious. The dry season here is from November to April each year, and the average temperature for the coldest month is 18.0 °C. The wet season here is from May to October, and the average temperature for the hottest month is 27.8 °C. The mean annual rainfall of 1100 mm (mainly concentrated in 7–10 months) [26]. The tropical karst landscapes of Hainan are located in the southernmost part of the central and western Hainan Island, with a total area of 400 km^2 consisting of exposed carbonate rocks [26], exposed bedrock, shallow soils, strong lithification, severe soil erosion, and highly heterogeneous habitats [26]. The tropical karst landscape of Hainan Island is characterized by a combination of homogeneous background areas and heterogeneous microhabitats with alternating wet and dry seasons [27]. Due to these seasonal changes, drought and infertile soils are the main stressors to plant growth and development in tropical karst habitats [28]. Compared to subtropical karst landscapes, the frequent alternation between heat and rain leads to significant moisture pulsation in tropical rainforest karst landscapes. As a result, strong leaching, erosion, and intense water evaporation all influence the formation of island karst rock gap habitats [29,30].

Impatiens hainanensis Y. L. Chen is a perennial herb endemic to Hainan Island's limestone regions and is only distributed in the karst tropical mountain rainforests at altitudes of 190–1300 m, in karst fissures [31] (Figure 1). *I. hainanensis* communities are dominated by low scrub and sparsely distributed with few species, often form dense rocky microhabitats, and limit their own regeneration and settlement due to the environment of rocky microhabitats [32]. Soil water in shallow karst fissures is an important water source for plants, and stone gap microhabitats indirectly affect vegetation growth by influencing soil water and nutrients [33,34]. Therefore, we hypothesized that *I. hainanensis* has a well-developed and dense root system that climbs rocks, penetrates fissures, and obtains water replenishment in fissured soils and karst crevices. During the rainy season (May to October, average rainfall is 1523 mm), due to increased precipitation, excess rainwater is stored in shallow karst fissures, and *I. hainanensis* may primarily rely on shallow water. During the dry season (November to April, average rainfall is 528 mm), as reduced precipitation reduces shallow soil water, *I. hainanensis* may shift their use of water from shallow soil water to deep soil water. Here, we investigate the water use of *I. hainanensis* in shallow rift habitats during the dry and wet seasons based on hydrogen and oxygen stable isotope techniques and ask the following questions: (1) What are the differences in water δD ($\delta^{18}O$) of *I. hainanensis* during the dry and wet seasons? (2) What is the impact of karst geological drought on water use in *I. hainanensis*? (3) What are the water-use strategies of *I. hainanensis* in a "soil-fissure" environment?



Figure 1. *Impatiens hainanensis* habitats. (**a**) Common habitats of *Impatiens hainanensis* in the wild; (**b**) *Impatiens hainanensis* karst fissure habitats.

2. Materials and Methods

2.1. Study Area and Locations

Our study area was located in the southwestern mountainous region of Hainan Island (in the southernmost part of mainland China). The Bawangling Emperor Cave of Changjiang County (Sample Plot A), the Exianling of Wangxia Township (Sample Plot B), and the Mihouling of Dongfang City (Sample Plot C) are typical tropical rainforest karst landscapes and belong to the tropical monsoon climate (Figure 2). As altitude increases, rainfall gradually increases, and relative humidity increases (mist and dew are often seen on the mountain). The geology of the study area primarily consists of limestone with intervals of metamorphic and sedimentary rocks [35]. Soil is mainly black or brown limestone. Soil cover is unevenly distributed, with the bedrock extensively exposed, steep slopes (63% of the slopes at $\geq 28^{\circ}$), thin soil layers, severe vegetation degradation, and low forest cover [35]. There was continuous outcrop of rocky habitat, including stone faces, caves, ditches, and crevices in each sample plot. The vegetation was mostly tropical evergreen

monsoon rainforest, deciduous monsoon rainforest, and hilltop scrub. The understory was rich in dead branches, while shrubs and groundcovers were growing vigorously. There was epikarst water in the vicinity of the sample sites and no surface streams passing through; thus we did not consider the effect of surface water on plant water-use sources.

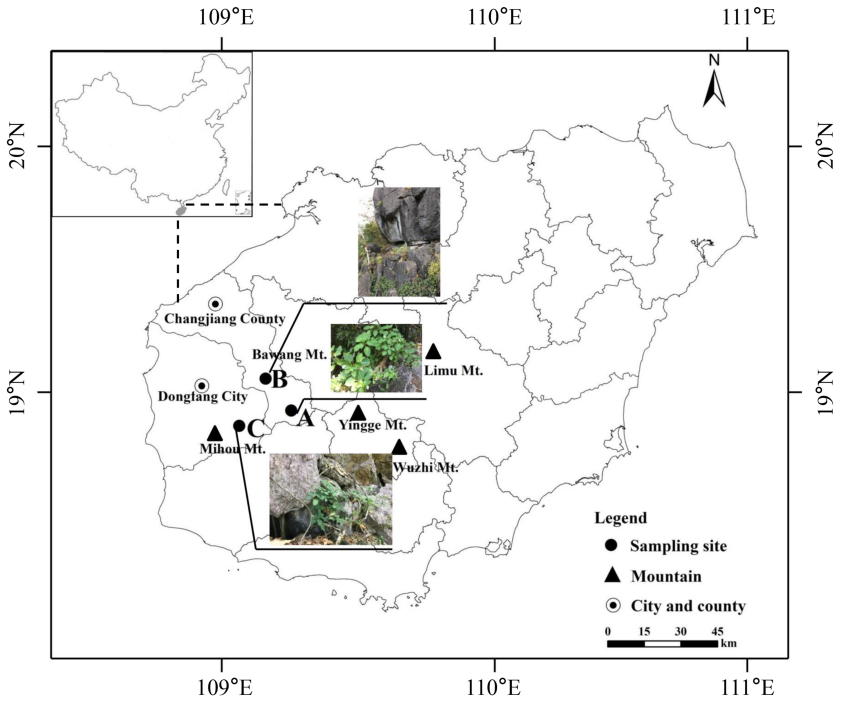


Figure 2. The location for our study site of *Impatiens hainanensis* on Hainan Island. (A, B, and C are the sampling plots for different *Impatiens hainanensis* populations. Each plot has nine repeated samples. Sample Plot A: Bawangling of Emperor Cave; Sample Plot B: Exianling; Sample Plot C: Mihouling).

2.2. Sample Collection

There were three *I. hainanensis* sample plots at the study site (Sample Plot A: Bawangling of Emperor's Cave, Sample Plot B: Exianling, Sample Plot C: Mihouling), and each sample plot was set up with nine repeated samples (5 m × 5 m). We collected samples from these sites, three times per month between 6 May 2018 and 6 April 2019. We collected stem bases from three mature *I. hainanensis* plants from each sample square (three replicates). We collected soil samples using a vertical soil profile by digging within each sample square at a distance from the sampling plants, and soil samples were collected at different depths (0–5 cm, 5–10 cm, 10–15 cm), with three replicates per layer. Standard rain gauges were set up at each sample site to collect rainwater after each rainfall. Nearby epikarst water was collected to represent the stable isotopic composition of the upper stagnant zone and the shallow groundwater in the area. Fog water was collected in the morning between 07:00 and 10:00 when the fog is thickest using collection tanks in the dry season. Sampling was divided between the wet season (May to October, 2018) and dry season (November 2018 to April 2019). Precipitation samples, epikarst water samples, stem water samples, soil water, and fog water collected in the field were quickly packed into sampling bottles, sealed with a sealing film to prevent evaporation, and stored in an incubator at −4 °C to be taken back to the laboratory.

2.3. Soil Water Content Determination

One 15 cm deep vertical soil profile was dug around each of the selected *I. hainanensis* in each sample square. Soil samples were collected at 0–5 cm, 5–10 cm, and 10–15 cm depths in aluminum boxes, with 3 replicates from each layer, and weighed in the laboratory. We dried the soil in an oven at 105 °C to a constant weight (measured every 24 h until the

weight remained constant) and weighed. We then calculated the water content of each layer of soil.

2.4. Investigation of Root Biomass

We selected nine well-grown *I. hainanensis* plants from each sample plot and collected the roots in layers by digging a soil profile around each plant. The root system was divided into three layers: 0–5 cm, 5–10 cm, and 10–15 cm. We then collected a volume of 4 cm × 4 cm × 4 cm from each soil layer, brought it back to the laboratory, crushed and sieved it, and then measured the root diameters with vernier calipers and graded according to fine (<1 mm), medium (1–2 mm), and coarse (>2 mm) roots. We weighted the fresh weight of the roots from each layer with an electronic balance, dried it at 75 °C in a drying oven to a constant weight (measured every 24 h until the weight remained constant), and then calculated the dry weight of the roots.

2.5. Stable Isotope Measurement

Soil water and stem water were extracted using evaporative cooling through a moisture vacuum extraction system (LI-2000). We used a Finnigan Delta V Advantage Isotope Ratio Mass Spectrometer (Thermo Fisher Scientific, Inc., USA) and Flash 2000 HT elemental analyzer measurements (±<1 ‰ for δD and ±<0.2 ‰ for $\delta^{18}O$) at the Flash, Stable Isotope Laboratory, Tsinghua University, to measure all water samples including atmospheric precipitation, soil water, epikarst water, and stem water samples. Hydrogen isotope ratios can be expressed in terms of the difference in thousands (‰) relative to the Vienna Standard Mean Ocean Water (V-SMOW) as follows:

$$\delta = (R_{\text{sample}}/R_{\text{standard}} - 1) \times 1000‰ \quad (1)$$

R_{sample} and R_{standard} are the $D/^{1}H$ and $^{18}O/^{16}O$ stable isotope compositions of the sample and V-SMOW [36,37].

2.6. Data Analyses

2.6.1. Utilization of Precipitation by Plants

Based on the δD value of the potential water source, we used the atmospheric precipitation and deep soil water (10–15 cm) as the two water-source ends of the plant to calculate the plant's uptake utilization at this precipitation using binary linear mixing model with the following equation:

$$P_p = \frac{\delta D_p - \delta D_{SW}}{\delta D_R - \delta D_{SW}} \times 100 \quad (2)$$

P_p is the proportion of plant water that is at the precipitation end of the scale, δD_R is the δD value of the water source at the precipitation, δD_{SW} is the δD value of the water source at the deep soil, and δD_p is the δD value of plant stem water.

2.6.2. Contribution of Precipitation to Soil Water

Using atmospheric precipitation and epikarst water as the two source ends of soil water, the contribution of precipitation to soil water in the layer was calculated using a binary linear mixing model with the following equation:

$$P_{sw} = \frac{\delta D_{SW} - \delta D_g}{\delta D_R - \delta D_g} \times 100 \quad (3)$$

P_{SW} represents the proportion of the water source at the precipitation in each layer of soil moisture, δD_R is the δD value of precipitation water sources, δD_R is the δD_g value of epikarst water sources, and δD_{SW} represents the δD value of soil water in each layer.

2.6.3. Plant Utilization of Soil Water at Different Depths

Isotopic values of stem water and potential water sources for each layer were substituted into the IsoSource model to calculate the proportion of soil water utilized by plants for each potential water source.

$$\delta X_p = \sum_{i=1}^{n} f_i \delta X_i, \quad (4)$$

δX_p is the δD and δ^{18}O values of stem water. δX_i is the δD and δ^{18}O values of the potential water source, and fi is the plant's utilization of the potential water sources.

2.6.4. Statistical Analysis

We used the statistical analysis software SPSS 26.0 for all data analysis. We conducted generalized linear model analyses to test the relationship between δD and δ^{18}O of atmospheric precipitation, plant stem water, and fog water. We used a mean comparison and ANOVA to compare the differences in δD and δ^{18}O between precipitation, plant, fog water, soil water in each layer, and epikarst water after different precipitation events in the wet and dry seasons. We used a multifactor ANOVA to test the effects of precipitation events, soil layers, and the contribution of precipitation to δD and δ^{18}O of soil water in each layer. All statistically significant differences were tested at 0.05 level.

3. Results

3.1. Dynamics of Atmospheric Precipitation

3.1.1. Dynamics of Atmospheric Precipitation δD (δ^{18}O) and Precipitation with Wet and Dry Season

The average annual rainfall in *I. hainanensis* habitat in 2018–2019 was 984 mm, with precipitation in 2018–2019 mainly concentrated in May to October (wet season), accounting for 82% of the annual precipitation, and the average annual evaporation was 1433 mm, 1.5 times the annual precipitation, with little variation in temperature from previous years (Figure 3). The hydrogen–oxygen isotope ratios for the atmospheric precipitation showed obvious seasonal differences in δD (δ^{18}O) values between dry and wet seasons at all three sample plots. During the wet season, the variation of δD (δ^{18}O) in the atmospheric precipitation is between −29.1 and −2.1‰, which is a relatively large variation. In the dry season, the variation of δD (δ^{18}O) in the atmospheric precipitation is between −11.8 and −4.9‰, which is a relatively small variation (Figure 4).

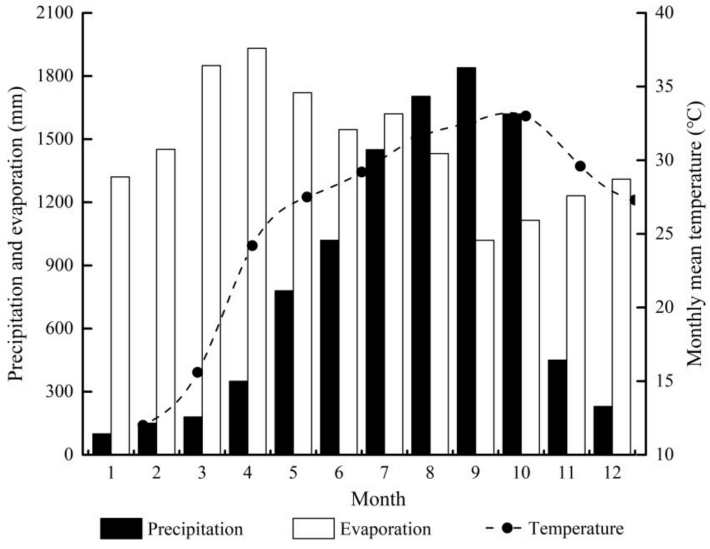


Figure 3. The monthly mean temperature, monthly precipitation, and monthly evaporation in *I. hainanensis* habitat during 2018–2019.

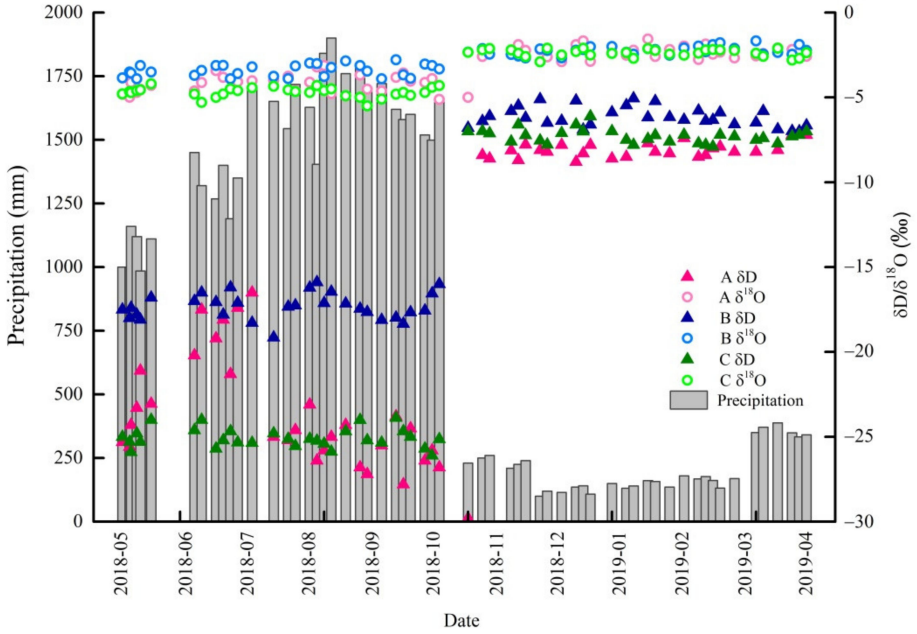


Figure 4. Dynamics of the atmospheric precipitation δD ($\delta^{18}O$) during the dry and wet season in the three sample plots (Sample Plot A: the Emperor Cave area of Bawangling; Sample Plot B: the Exianling area; Sample Plot C: the Mihouling area; wet season: May to October, 2018; dry season: November 2018 to April 2019).

3.1.2. Atmospheric Precipitation δD ($\delta^{18}O$) Characteristics

According to the relationship diagram of δD ($\delta^{18}O$) for all three sample plots (Figure 5), the local meteoric water line (LMWL) deviates from the global meteoric water line (GMWL) to different degrees due to seasonal differences in moisture sources and moisture factors. The one-variable linear regression analysis of δD on $\delta^{18}O$ for atmospheric precipitation showed that the slope in the equation for the atmospheric precipitation line at the study sample sites was small and the intercept was large during the wet season compared with the global atmospheric precipitation line. It also showed that the slope and intercept in the equation for the atmospheric precipitation line were both small during the dry season. The slope and intercept of the atmospheric precipitation line equation are smaller in the dry season than when compared with the wet season. This indicates that the air humidity in the *I. hainanensis* sample plots is relatively low due to local precipitation and that there is a certain degree of evaporation.

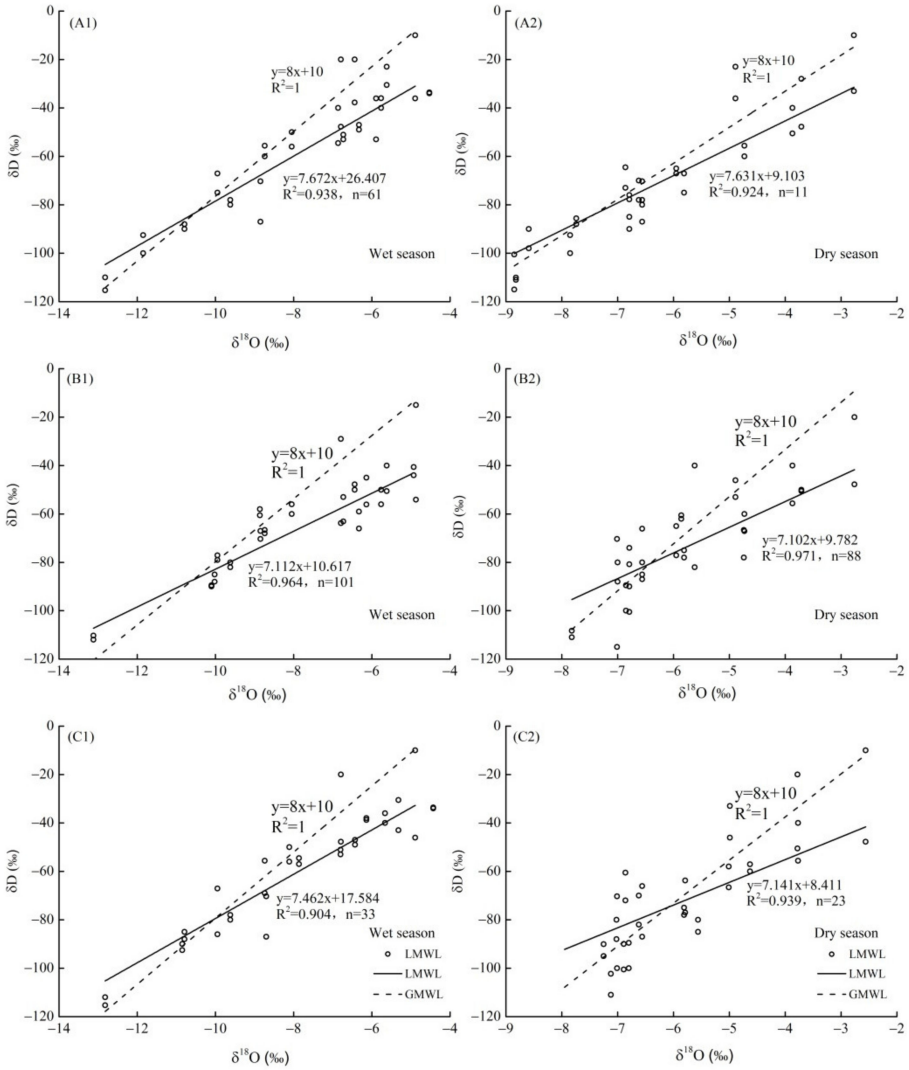


Figure 5. Linear relationship between δD ($\delta^{18}O$) of atmospheric precipitation of *I. hainanensis* during the wet season (**left**) and dry season (**right**). (**A1**) The Emperor Cave area in the wet season; (**B1**) the Exianling area in the wet season; (**C1**) the Mihouling area in the wet season. (**A2**) the Emperor Cave area in the dry season; (**B2**) the Exianling area in the dry season; (**C2**) the Mihouling area in the wet season. LMWL: the local meteoric water line, GMWL: the global meteoric water line.

3.2. Dynamics of Soil Water

3.2.1. Changes of Soil Water Content

During the dry season, the variation in soil water content ranged from 14.1 to 19.8% in Sample Plot A, from 18.6 to 26.5% in Sample Plot B, and from 16.3 to 19.4% in Sample Plot C (Figure 6). Soil water content of the 0–5 cm surface layer is affected by evaporation less than the soil water content at the 5–10 cm and 10–15 cm depths, and the soil water content gradually increases with increasing soil depth. During the wet season, the variation of soil water content in Sample Plot A ranges from 45.2 to 33.1%, the variation of soil water content in Sample Plot B ranges from 42.2 to 27.3%, and the soil water content in Sample Plot C ranges from 45.1 to 30.2%. The soil moisture content in the 0–5 cm surface layer is higher than at the 5–10 cm and 10–15 cm depths due to the influence of precipitation in the wet season, and the soil moisture content gradually decreases with increasing soil depth. Overall, soil moisture content is significantly higher in the wet season than in the dry season.

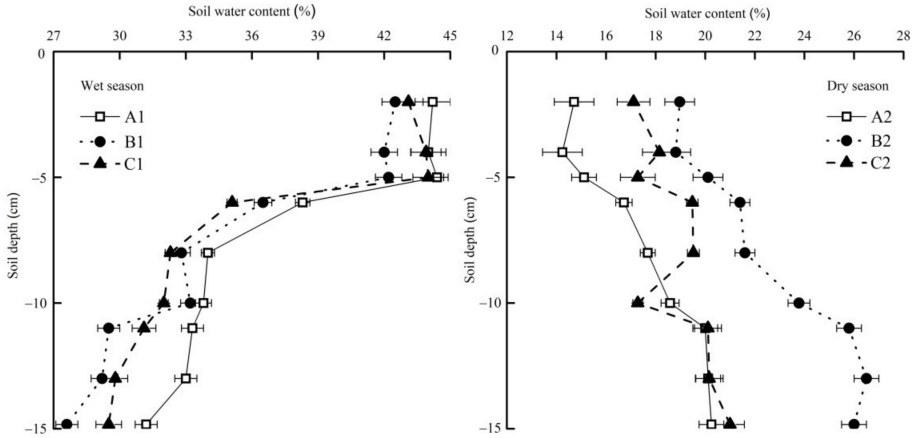


Figure 6. Dynamics of soil water content (mean ± SD, n = 9) in each layer during the dry and wet seasons. (**A1**) The Emperor Cave area in the wet season; (**B1**) the Exianling area in the wet season; (**C1**) the Mihouling area in the wet season. (**A2**) the Emperor Cave area in the dry season; (**B2**) the Exianling area in the dry season; (**C2**) the Mihouling area in the wet season.

3.2.2. Dynamics of Soil Water δD ($\delta^{18}O$) with Soil Depth

In the wet season, soil water δD ($\delta^{18}O$) values vary widely at depths of 0–10 cm, indicating that precipitation in the wet season can quickly reach these depths. Soil water δD ($\delta^{18}O$) values begin to shift to the right at depths of 0–5 cm and continue to shift to the right at 5–10 cm. At depths of 10–15 cm δD ($\delta^{18}O$), values begin to decrease and eventually stabilize. In the dry season, soil water δD ($\delta^{18}O$) values at depths of 0–15 cm change more, indicating that precipitation in the dry season could quickly reach depths of 0–15 cm. The δD ($\delta^{18}O$) value of soil water at the depth of 0–5 cm shifted to the right, continued shifting to the right at 5–10 cm, and then shifted to the left at 10–15 cm, indicating that the δD ($\delta^{18}O$) value of precipitation in the dry season changed significantly and precipitation gradually penetrated into the deep soil of 10–15 cm from 0–5 cm (Figure 7).

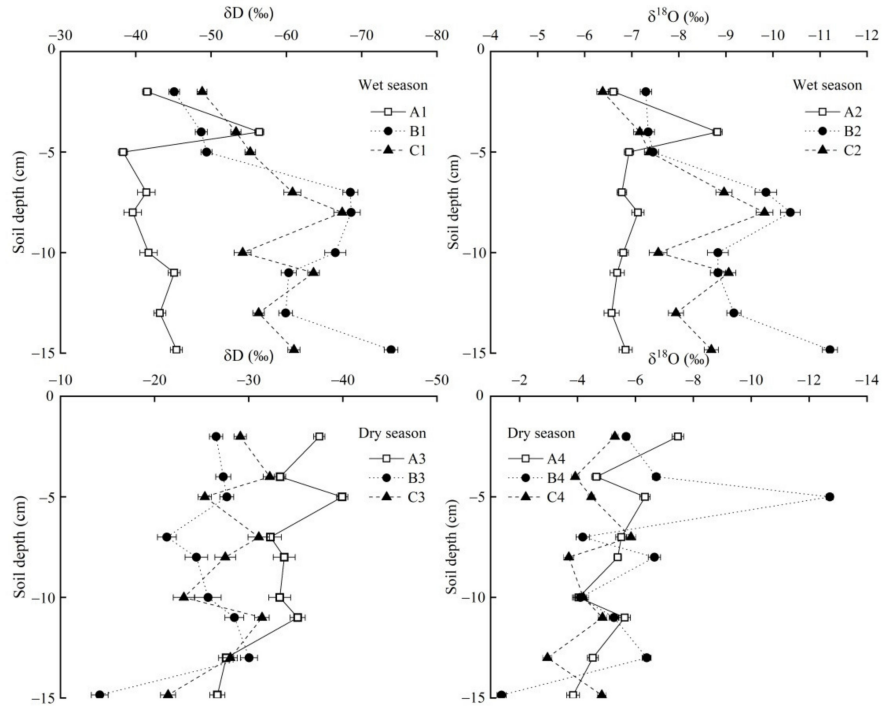


Figure 7. Dynamics of soil water δD ($\delta^{18}O$) (mean ± SD, n = 9) with soil depth under different precipitation conditions in wet season and dry season. (**A1**) Dynamics of soil water δD in the Emperor

Cave area during the wet season; (**B1**) dynamics of soil water δD in the the Exianling area during the wet season; (**C1**) dynamics of soil water δD in the Mihouling area during the wet season. (**A2**) dynamics of soil water $\delta^{18}O$ in the Emperor Cave area during the wet season; (**B2**) dynamics of soil water $\delta^{18}O$ in the Exianling area during the wet season; (**C2**) dynamics of soil water $\delta^{18}O$ in the Mihouling area during the wet season. (**A3**) dynamics of soil water δD in the Emperor Cave area during the dry season; (**B3**) dynamics of soil water δD in the Exianling area during the dry season; (**C3**) dynamics of soil water δD in the Mihouling area duing the dry season. (**A4**) dynamics of soil water $\delta^{18}O$ in the Emperor Cave area during the dry season; (**B4**) dynamics of soil water $\delta^{18}O$ in the Exianling area during the dry season; (**C4**) dynamics of soil water $\delta^{18}O$ in the Mihouling area during the dry season.

3.2.3. Contribution of Precipitation to Soil Water at All Levels

During the wet season, the highest contribution of precipitation to soil water in the 0–5 cm surface layer was between 58.1 and 78.5%, and the higher the amount of precipitation, the higher the contribution of precipitation to soil water at the 0–5 cm surface layer. The contribution of precipitation to soil water in each layer decreased gradually with the increasing soil depth. In the dry season, the contribution of precipitation to soil water in the deep layer of 10–15 cm was between 55.2 and 77.4% at the highest point, the contribution to soil water in the surface layer at the 0–5 cm depth was only 26–46%, and the contribution of precipitation to soil water in each layer gradually increased as the soil depth increased (Figure 8).

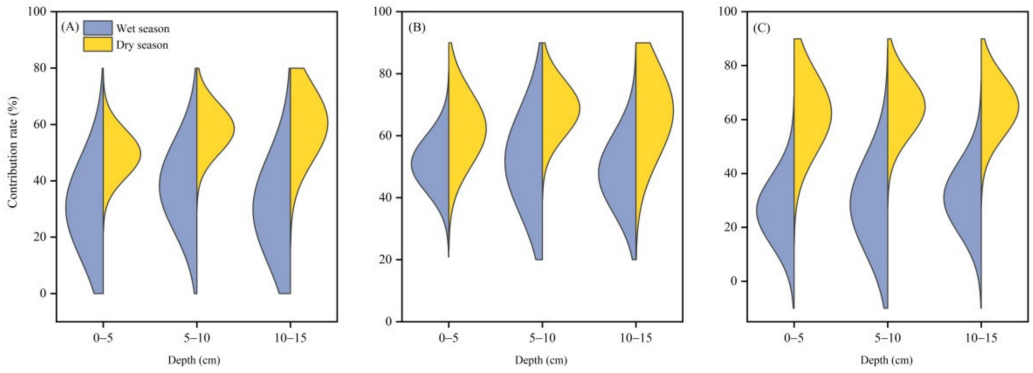


Figure 8. Contribution of precipitation to soil water in each layer. (**A**) The Emperor Cave area; (**B**) the Exianling area; (**C**) the Mihouling area.

3.3. Dynamics of Plant Stem Water

3.3.1. Vertical Distribution of Roots

The vertical distribution of root biomass (i.e., the percentages of coarse, medium, and fine roots in each layer of soil in the total root biomass) of *I. hainanensis* for the three sample sites is shown in Figure 9. The biomass of fine roots accounted for 65.2% of the total root biomass, and the biomass of coarse roots (>2 mm) was mainly distributed at the 0–5 cm depth of surface soil and accounted for 64.8% of the total root biomass. The proportion of fine root biomass increased with the increasing of soil depth, and the proportion of coarse root biomass decreased with the increasing soil depth. During the wet season, the fine roots ($\leq$1 mm) of *I. hainanensis* were mainly distributed at 10–15 cm deep soil and accounted for 55.6% of the total root biomass, while the coarse roots (>2 mm) were mainly distributed at 0–5 cm surface soil and accounted for 60.3% of the total root biomass. During the dry season, coarse root biomass accounted for 23.7% more of the total root biomass than coarse root biomass in the wet season. During the wet season, the proportion of fine root biomass from the total root biomass of *I. hainanensis* was 20.3% less than that of the dry season.

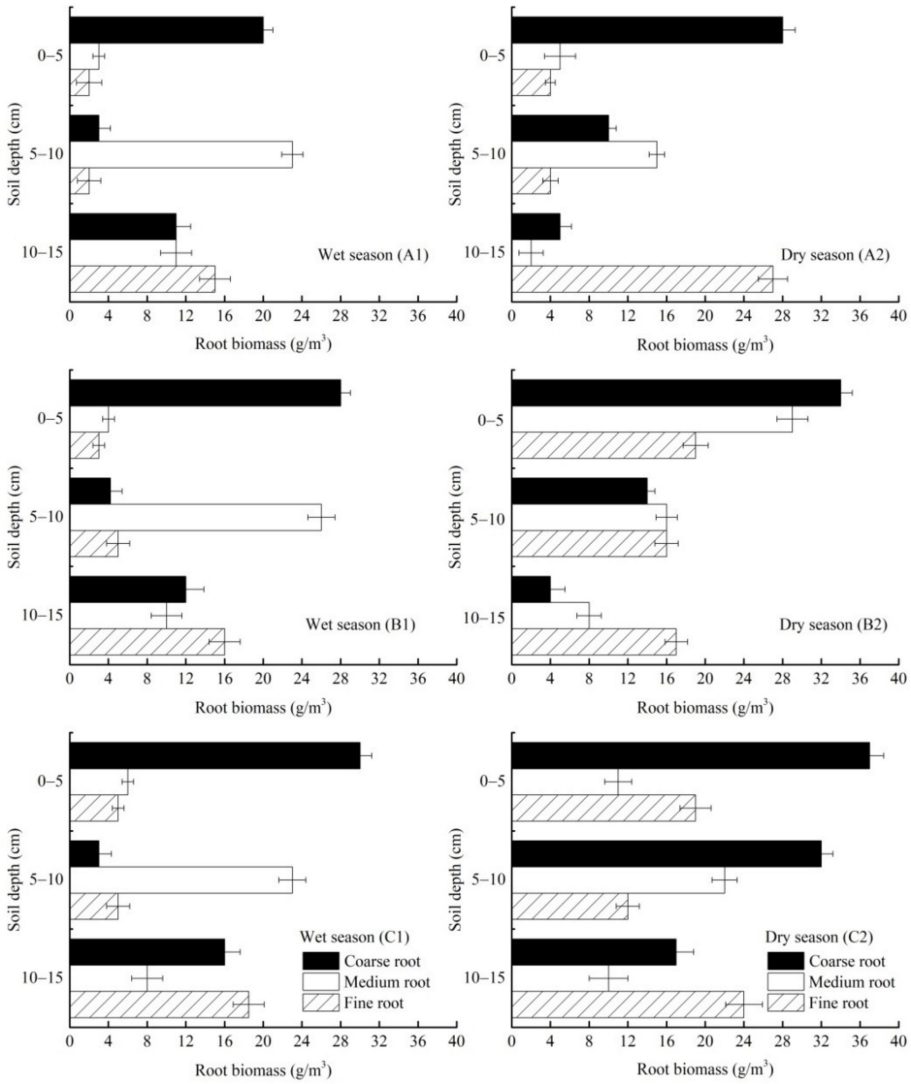


Figure 9. Vertical distribution of root biomass of *I. hainanensis* in the wet (**left**) and dry seasons (**right**) ($p < 0.05$). (**A1**) Vertical distribution of root biomass in the Emperor Cave area during the wet season; (**B1**) vertical distribution of root biomass in the Exianling area during the wet season; (**C1**) vertical distribution of root biomass in the Mihouling area during the wet season. (**A2**) vertical distribution of root biomass in the Emperor Cave area during the dry season; (**B2**) vertical distribution of root biomass in the Exianling area during the dry season; (**C2**) vertical distribution of root biomass in the Mihouling area during the dry season. (Fine root: a $\leq$ 1 mm, Medium root: 1 mm< a $\leq$ 2 mm, Coarse root: a > 2 mm.)

3.3.2. Relationship between Plant Stem Water δD and Soil Water δD

The stem water δD of the three *I. hainanensis* sample plots ranged consisted of precipitation δD and soil water δD (Figures 10 and 11), indicating that *I. hainanensis* utilized both atmospheric precipitation and components from other water sources (e.g., soil water, etc.) with precipitation changes associated with changes from the wet to the dry season. During the wet season, the utilization rates of soil water for *I. hainanensis* at Sample Plot A were 68.2% (0–5 cm), 29.8% (5–10 cm), and 2% (10–15 cm). The utilization rates of soil water for Sample Plot B were 51.2% (0–5 cm), 40.8% (5–10 cm), and 8% (10–15 cm). The utilization rates of soil water for Sample Plot C were 59.5% (0–5 cm), 37.8% (5–10 cm), and 2.7% (10–15 cm). These rates indicate that stem water was mainly utilized by soil water at depths of 0–5 cm and 5–10 cm and that the average utilization rates were 59.6% and 36.1%. During the dry season, the utilization rates for Sample Plot A were 8.9% (0–5 cm), 13.8%

(5–10 cm), and 77.3% (10–15 cm). The utilization rates for Sample Plot B were 3.4% (0–5 cm), 14.1% (5–10 cm), and 82.5% (10–15 cm). For Sample Plot C, they were 7.5% (0–5 cm), 19.7% (5–10 cm), and 72.8% (10–15 cm). This indicates that the stem water mainly utilized the deep soil water, with an average utilization rate of 77.5% and a maximum utilization rate of 82.5%. In particular, the average utilization rate of soil water by *I. hainanensis* for 0–5 cm and 5–10 cm dropped sharply to 6.6% and 15.9%, respectively.

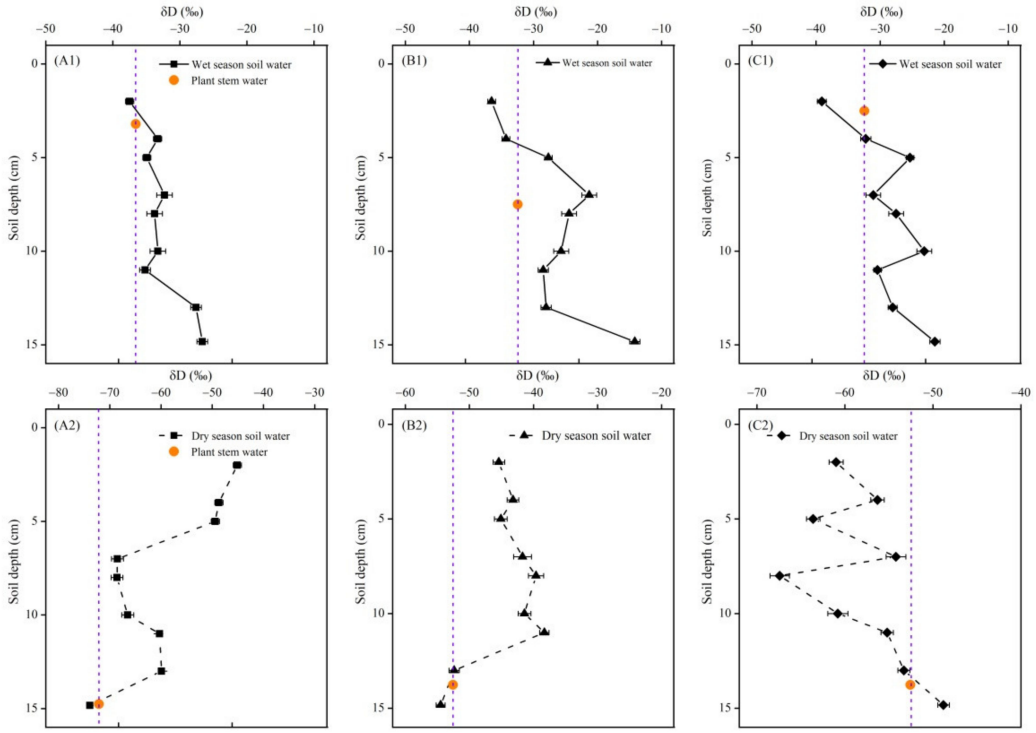


Figure 10. Relationship between stem water δD and soil water δD (mean ± SD, $n = 9$) of *I. hainanensis*. (**A1**) The Emperor Cave area in the wet season; (**B1**) the Exianling area in the wet season; (**C1**) the Mihouling area in the wet season. (**A2**) the Emperor Cave area in the dry season; (**B2**) the Exianling area in the dry season; (**C2**) the Mihouling area in the dry season.

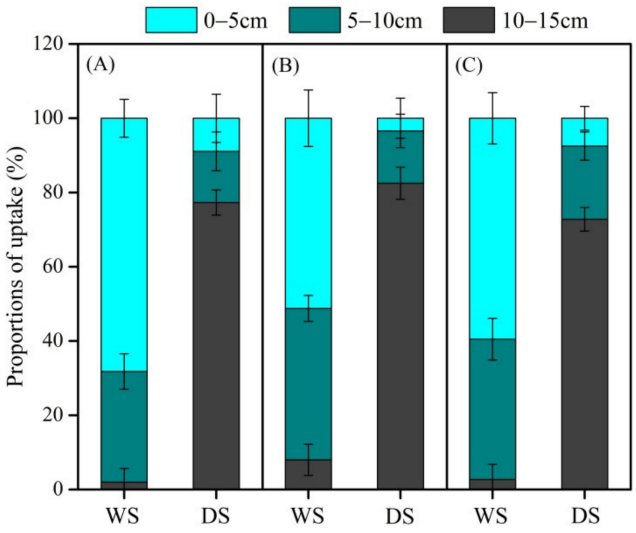


Figure 11. Utilization of soil water at different depths by *I. hainanensis* ($p < 0.05$). (**A**) The Emperor Cave area; (**B**) the Exianling area; (**C**) the Mihouling area. WS: wet season, DS: dry season.

3.3.3. Utilization of Dry and Wet Season Precipitation by *I. hainanensis*

The utilization rate of *I. hainanensis* to different precipitation conditions during the wet and dry seasons is shown in Figure 12. In the wet season, the utilization rate of *I. hainanensis* for precipitation in sample plots A, B, and C ranged from 60.1 to 86.3%, 62.1 to 76.6%, and 65.2 to 75.8%. In the dry season, the utilization rate of *I. hainanensis* for precipitation in sample plots A, B, and C ranged from 50.3 to 68.2%, 22.2 to 38.6%, and 33.4 to 58.5%. Compared to the wet season, *I. hainanensis* use more precipitation than the dry season. The response of *I. hainanensis* to wet season precipitation is more rapid and highly utilized.

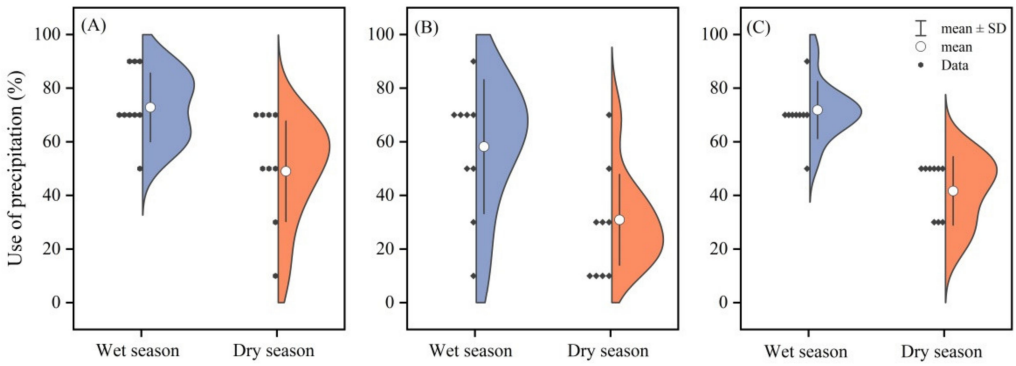


Figure 12. Utilization of rainfall in dry and wet seasons by *I. hainanensis*. (**A**) The Emperor Cave area; (**B**) the Exianling area; (**C**) the Mihouling area.

3.4. Dynamics of Fog Water

A linear regression analysis of fog water δD and $\delta^{18}O$ in the *I. hainanensis* showed that the linear correlation between soil water δD and $\delta^{18}O$ was highly significant (Figure 13). This indicates that *I. hainanensis* were able to utilize both atmospheric precipitation and other water sources (e.g., fog water) in the area. During the dry season, fog water δD and plant water δD are closely related (Figure 14), indicating that *I. hainanensis* take up and use fog water. Fog water has a partial water recharge effect on *I. hainanensis* in the dry season.

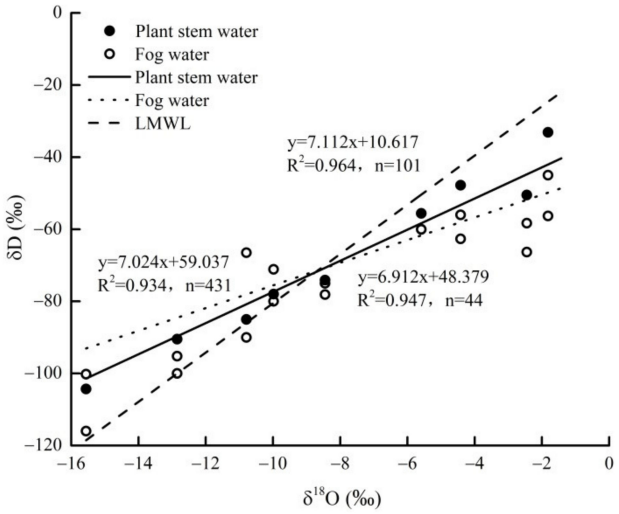


Figure 13. The correlation between δD and $\delta^{18}O$ of plant stem water.

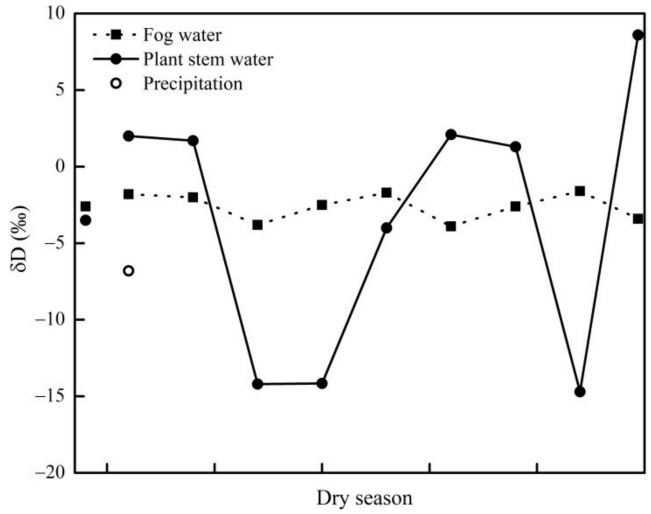


Figure 14. Changes in δD values of fog water, precipitation, and stem water with dry season precipitation.

3.5. Relationship of Epikarst Water to Precipitation, Soil Water, Stem Water, and Fog Water

Figure 15 shows a graph with the relationship between epikarst water δD ($\delta^{18}O$) and atmospheric precipitation δD ($\delta^{18}O$), soil water δD ($\delta^{18}O$), and stem water δD ($\delta^{18}O$). During the wet season, the δD ($\delta^{18}O$) values of stem water, soil water, and epikarst water are very close to the regional and global precipitation line, which indicates that stem water, soil water, and epikarst water mainly came from atmospheric precipitation. The close relationship between the δD of epikarst water and the δD of local precipitation in the wet season indicates that atmospheric precipitation is the main source of epikarst water. The values of epikarst water δD ($\delta^{18}O$) were also close to the regional precipitation line and the values of stem water and soil water. This also indicates that *I. hainanensis* absorbs epikarst water as well as atmospheric precipitation and soil water in this region.

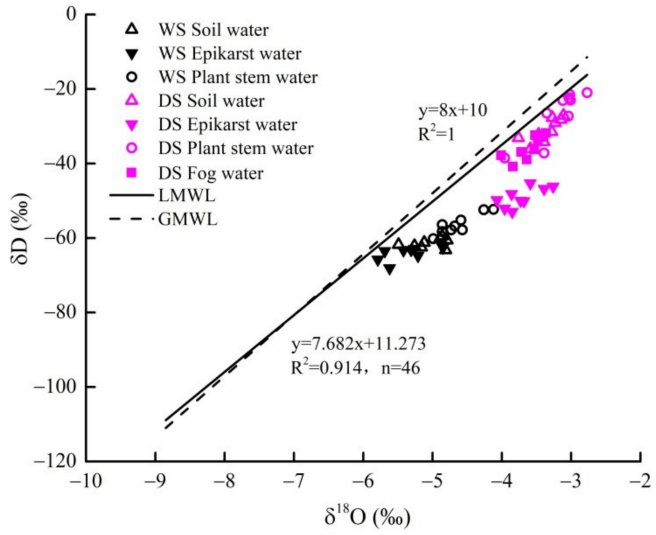


Figure 15. Linear relationship between δD($\delta^{18}O$) for each water (each water includes soil water, epikarst water, plant stem water, and fog water; LMWL: the local meteoric water line, GMWL: the global meteoric water line).

During the dry season, atmospheric precipitation has less influence on the δD of epikarst water. Additionally, the δD ($\delta^{18}O$) values for plant water, soil water, and fog water were close to the regional and global precipitation lines when compared with epikarst water. This indicates that plant and soil water of *I. hainanensis* is mainly derived from atmospheric

precipitation and fog water. During the wet season, the increase in precipitation leads to the epikarst water level rising, and the deep soil receives rising recharge from epikarst water in addition to recharge from precipitation. In the dry season, there was little recharge from epikarst water to the soil. In both the wet and dry seasons, soil filling makes the shallow karst fissures a major channel for subsurface leakage and the main soil-supporting space for karst areas. Soil filling in shallow karst fissures slows down the rate of water infiltration and leakage to a certain extent, and *I. hainanensis* take advantage of this unique microhabitat to absorb sufficient water to sustain themselves in karst fissures.

4. Discussion

4.1. Differences in Moisture Sources of I. hainanensis during the Wet and Dry Seasons

The δD ($\delta^{18}O$) values for the atmospheric precipitation in the *I. hainanensis* sample plots were smaller when compared with global atmospheric precipitation δD ($\delta^{18}O$) values. This indicates that because of the influence of the tropical monsoon climate and high precipitation, the fractionation of hydrogen and oxygen isotopes in precipitation is smaller in these sample plots when compared with other regions. The seasonal precipitation variation makes the hydrogen–oxygen isotope fractionation during precipitation less obvious, and there is a close correlation between the hydrogen–oxygen isotope composition of precipitation and various environmental factors such as season [38–41]. The results from this study show that the isotopic composition of atmospheric precipitation in the *I. hainanensis* sample plots was correlated with precipitation (i.e., there was a significant precipitation effect), which may be caused by differences in the main water vapor sources between the wet and dry seasons in the *I. hainanensis* sample plot. In the wet season, the δD values of plant water of *I. hainanensis* ranged between the δD values of shallow and middle soil water and the δD values of epikarst water, indicating that plant water of *I. hainanensis* mainly came from soil water and epikarst water. During the dry season, the δD values of *I. hainanensis* plant water were between the δD values of atmospheric precipitation and deep soil water, indicating that *I. hainanensis* plant water mainly came from precipitation and deep soil water. In this study, the utilization of shallow and middle soil water by *I. hainanensis* reached 59.6% and 36.1% in the wet season, while in the dry season, the utilization of middle and deep soil water by *I. hainanensis* reached 15.9% and 77.5%. This difference in water use reflects the functional characteristics of the soil type and the community structure of *I. hainanensis* in shallow karst rift habitats, as well as the adaptation of *I. hainanensis* to different water conditions between the dry and wet seasons. The temporal and spatial dynamics of soil water δD are influenced by differences in precipitation δD and precipitation magnitudes, which are dependent on the intensity of precipitation and evaporation of soil water δD values and infiltration [42–45]. In the wet season, soil water δD values were in between precipitation values and epikarst water values. This indicates that the soil water in the *I. hainanensis* sample plots was mainly derived from atmospheric precipitation and epikarst water. As the intensity of precipitation increases during the wet season, the rate of water displacement in the soil becomes faster, leading to faster infiltration of precipitation into the soil, and influencing the precipitation on the soil to become more pronounced. In the wet season, the rise in the epikarst karst water level causes the deep soil water and epikarst water to be recharged by atmospheric precipitation. In the dry season, the epikarst water level decreases, the recharge of soil water mainly comes from atmospheric precipitation, the surface soil water is recharged of soil water, and surface soil water mainly comes from atmospheric precipitation. Surface soil water is affected by evaporation and precipitation, resulting in an increased evaporation rate, which is often subject to drought stress [46–50], and is consistent with the findings of Xu et al. [51]. As precipitation increases, the rate of infiltration of precipitation from the soil surface to the deeper soil layers accelerates, the effect on deep soil water δD becomes more obvious, and the contribution of precipitation to soil water gradually increases.

4.2. Effect of Karst Drought on Water Use of I. hainanensis

During the dry season when precipitation is low and there is an insufficient water supply at the shallow layer, *I. hainanensis* mainly use stable deep water, water from shallow fissures, and fog water. This results in *I. hainanensis* distributing more coarse and fine roots when compared with the wet season when plants accelerate water uptake and use. Plants such as *Cyclobalanopsis glaucoides* and *Pistacia weinmannifolia* in karst areas also use more deep soil water in the dry season and switch to medium soil water in the wet season [52]. Plants will preferentially use water stored in the surface soil and shallow fissures when rainfall is relatively abundant and recharge the aquifers below the surface, which reduces the energy used to absorb water and promotes plant growth [53–57]. In addition, high-altitude karst areas are foggy in the dry season, with strong transpiration and high plant water demand, soil water cannot be supplied to the plants in time, and thus *I. hainanensis* use some of the fog water to increase their own water-use efficiency and reduce plant transpiration water loss.

During the wet season, precipitation is adequate, soil water is effectively recharged, water-use layers are close together, soil water is mainly concentrated in the shallow and middle layers, and *I. hainanensis* turns to the short-term available water in the shallow and middle layers. Related studies have shown that the source of water for perennial desert succulents in arid desert environments is deep soil water or groundwater, with other annuals with shallow roots using shallow groundwater recharged by precipitation [57]. This is similar to the fact that *I. hainanensis* mainly use deep soil water in the dry season, and some plants in arid areas shift from mainly absorbing deep soil water or groundwater to mainly absorbing shallow soil water recharged by rainfall with the onset of the rainy season and in areas with abundant precipitation may also develop upper and lower double root systems, using both deep and shallow soil water [58]. However, considering the specific geology of karst and desert areas, local plants use water not only from soil water but also deep groundwater in the rainy season for desert plants, while karst plants also use shallow fissure water and surface karst water, and even fog water due to climatic factors [59]. Plants in different arid ecosystems also develop different water-use strategies to adapt to the different local habitats. The different sources of water use in the wet and dry seasons of *I. hainanensis* reflect both similar water-use patterns to those of plants in arid regions, while at the same time showing local adaptation mechanisms to tropical karst seasonal precipitation and moisture environments.

4.3. Water Utilization of I. hainanensis under "Fissure-Soil" Habitat Characteristics

Plants can respond to changes in their environment with changes to morphology, physiology, and other characteristics that allow them to exhibit certain functional strategies [60–62]. Plants in karst regions have strong root systems, lithogenic, penetrating fissures, climbing rocks, and even roots encasing rocks to find water and nutrients in rock fissures and surface karst zones [63,64]. In this study, the coarse roots (>2 mm) of *I. hainanensis* were mainly distributed at the 0–5 cm surface layer of soil and accounted for 64.8% of the total root biomass in the dry season, while the fine roots (<1 mm) were concentrated at the 10–15 cm deep layer of soil and accounted for 65.2% of the total fine root biomass. Compared with the dry season, the coarse roots (>2 mm) and fine roots (<1 mm) of *I. hainanensis* in the wet season were less distributed in both surface and deep layer soil. The distribution of coarse roots (>2 mm) and fine roots (<1 mm) was lower in both topsoil and deep soil layers when compared with the dry season. Differences in plant strategies between the wet and dry seasons lead to different distributions of fine and coarse roots. Differences in root biomass distribution determined the ability of these plants to absorb and utilize soil water and the extent they can take up nutrients [25,65].

The depth of root distribution of desert plants is related to the location of the soil water used by plans [66,67]. Shallow-rooted plants are sensitive to precipitation and have a high capacity to use shallow soil water, but rainfall tends to evaporate, and shallow soil moisture is very variable; deep-rooted plants can penetrate several meters below the

soil [68]. Many perennial plants in semi-arid and seasonally dry areas have dimorphic root systems that can use upper soil water in the wet season and take up deep soil water in the dry season [69]. In contrast, the root distribution depth of some plants in the karst area is related to the location of soil water, different seasonal root distribution strategies for water uptake, and utilization under the influence of alternating wet and dry seasons. In the dry season, *I. hainanensis* mainly utilized part of the precipitation and deep soil water. This indicates that soil water stored in shallow karst fissure water was the main source of plant stem water during this time. Due to the bare rocks in the *I. hainanensis* habitat, the surface soil moisture decreased and leaked severely, increase of plant coarse root distribution was more conducive to *I. hainanensis* climbing rocks and absorbing water deep into the shallow fissured soil, and the water absorption was more relatively concentrated. Shallow karst fissure water became a secondary water source for plant water utilization [70–72]. In the wet season, the increase in the distribution of fine roots also leads to an increase in the capacity for *I. hainanensis* to absorb and utilize soil water and the plant's range of water uptake. *I. hainanensis* mainly utilized part of the precipitation, shallow, and middle soil water. This indicates that *I. hainanensis* has reduced the use of shallow karst fissure water in favor of surface soil; however, shallow karst fissure water is still the main source of water for plants. The water content of surface soils on karst slopes declines rapidly after rainfall, while precipitation infiltrates into shallow fissures soils and remains stored in the shallow fissures for a long time. Shallow fissures are an important part of the surface karst zone and the main way of subsurface leakage for karst slope soils. Therefore, shallow karst fissures serve as the "container" for soil storage in special karst habitats [73,74]. The "fissure-soil" system makes the shallow karst fissures not only a pathway for subsurface soil leakage but also provides roots the space, water, and nutrients needed for growth. The "fissure-soil" system changes the water process in karst slope, with fissured soil slowing the infiltration rate of fissured water, and stores some water in the soil [26,27,75]. The "fissure-soil" system plays an important ecological function in supporting karst ecosystems and regulating hydrological processes.

5. Conclusions

In this study, we used stable isotope techniques to analyze the seasonal variation of water sources in the dry and wet seasons of *I. hainanensis* in a karst "fissure-soil" habitat. In the wet season, the main water sources of *I. hainanensis* were shallow and middle soil water, shallow karst fissure water, and epikarst water. Among them, the *I. hainanensis* in the Emperor Cave area was relatively more affected by the precipitation in the wet season when compared with the other two sample plots. Response was faster, and the utilization rate was higher, which may be related to the fact that this sample plot is located at the foot of the mountain, the slope is gentle, the soil thickness is larger, and the gravel content is lower. In the dry season, *I. hainanensis* uses deep soil water and shallow karst fissure water for its main water sources. As precipitation decreases and evaporation increases, most of the precipitation is lost through soil evaporation, surface run-off, and leakage, and precipitation becomes invalid. Most of the water in the shallow fissures is consumed, and only a small part is stored in the shallow fissures filled with litter and organic matter. The effective water in the soil layer decreases rapidly, and the effective water in the epikarst zone also slowly weakens. In the contiguous rocky habitats in the karst area, shallow karst fissures provide space for soil and growth space for plant roots, forming a "fissure-soil-plant" system. *I. hainanensis* has formed a water-use mode dominated by shallow karst fissure water. This shallow karst fissure water can help the *I. hainanensis* community maintain water consumption and can allow us to forecast the water-use strategies for this plant in this habitat under changes between the wet and dry seasons.

Author Contributions: Study conception and design, W.H. and X.S.; investigation, W.H. and C.Z.; data collection, W.H. and C.Z.; data analysis and interpretation of results, W.H. and Y.Z.; draft manuscript preparation, W.H., M.R. and Y.D.; manuscript revision, W.H. and Y.D. All authors have read and agreed to the published version of the manuscript.

Funding: This research was jointly supported by (1) the National Natural Science Foundation of China (Grant No. 31560229); (2) Hainan Provincial Graduate Innovation Research Project (Grant No. Hyb2017-27); and (3) Hainan University Research Project (Grant No. KYQD (ZR) 20055).

Institutional Review Board Statement: Not applicable.

Informed Consent Statement: Not applicable.

Data Availability Statement: Not applicable.

Acknowledgments: We thank Wang Jingjing and Meng Xinya from the college of Forestry, Hainan University, for her valuable comments on the writing of this paper. We also thank Zhao Moqiang, a ranger at the Bawangling National Nature Reserve, for his assistance in the field. We would like to thank Henry Camarillo for his assistance with English language and grammatical editing.

Conflicts of Interest: The authors declare no conflict of interest.

References

1. Asbjornsen, H.; Goldsmith, G.R.; Alvarado-Barrientos, M.S.; Rebel, K.; Van Osch, F.P.; Rietkerk, M.; Chen, J.; Gotsch, S.; Tobon, C.; Geissert, D.R.; et al. Ecohydrological advances and applications inplant-water relations research: A review. *J. Plant Ecol.* **2011**, *4*, 3–22. [CrossRef]
2. Zeppel, M. Convergence of tree water use and hydraulic architecture in water-limited regions: A review and synthesis. *Ecohydrology* **2013**, *6*, 889–900. [CrossRef]
3. Drake, P.L.; Franks, P.J. Water resource partitioning, stem xylem hydraulic properties, and plant water use strategies in a seasonally dry riparian tropical rainforest. *Oecologia* **2003**, *137*, 321–329. [CrossRef]
4. Liu, J.R.; Song, X.F.; Yuan, G.F.; Sun, X.M.; Liu, X.; Wang, S.Q. Characteristics of $\delta^{18}O$ in precipitation over Eastern Monsoon China and the water vapor sources. *Chin. Sci. Bull.* **2010**, *55*, 200–211. [CrossRef]
5. Liu, W.J.; Liu, W.Y.; Li, P.J.; Duan, W.P.; Li, H.M. Dry season water uptake by two dominant canopy tree species in a tropical seasonal rainforest of Xishuangbanna, SW China. *Agr. Forest Meteorol.* **2010**, *150*, 380–388. [CrossRef]
6. Xu, Q.; Li, H.B.; Chen, J.Q.; Cheng, X.L.; Liu, S.R.; An, S.Q. Water use patterns of three species in subalpine forest, Southwest China: The deuterium isotope approach. *Ecohydrology* **2011**, *4*, 236–244. [CrossRef]
7. Williams, D.G.; Ehleringer, J.R. Intra-and Interspecific Variation for Summer Precipitation Use in Pinyon-Juniper Woodlands. *Ecol. Monogr.* **2000**, *70*, 517–537.
8. Ehleringer, J.R.; Sage, R.F.; Flanagan, L.B.; Pearcy, R.W. Climate change and evotion of C4 photosynthesis. *Trends Ecol. Evol.* **2010**, *6*, 95–99. [CrossRef]
9. Xu, Q.; Ji, C.L.; Wang, H.Y.; Li, C. Use of Stable Isotopes of Hydrogen, Oxygen and Carbon to Identify Water Use Strategy by Plants. *World For. Res.* **2009**, *22*, 41–46.
10. Ehleringer, J.R. Variation in leaf carbon isotope discrimination in Encelia farinose: Implications for growth, competition, and drought survival. *Oecologia* **2013**, *95*, 340–346. [CrossRef] [PubMed]
11. Pergo, É.M.; Ishii-Iwamoto, E.L. Changes in energy metabolism and antioxidant defense systems during seed germination of the weed species ipomoea triloba L. and the responses to allelochemicals. *J. Chem. Ecol.* **2011**, *37*, 500–513. [CrossRef] [PubMed]
12. Smedley, M.P.; Dawson, T.E.; Comstock, J.P.; Donovan, L.A.; Sherrill, D.E.; Cook, C.S.; Ehleringer, J.R. Seasonal carbon isotope discrimination a grassland community. *Oecologia* **2011**, *85*, 314–320. [CrossRef]
13. Xu, Q.; Liu, S.R.; An, S.Q.; Jiang, Y.X.; Wang, Z.S.; Liu, J.T. Allocation of precipitation in a Sub-Alpine dark coniferous forest of western SiChuan using stable oxygen isotopes. *Chin. J. Plant Ecol.* **2006**, *30*, 83–89.
14. Richter, D.D.; Billings, S.A. 'One physical system': Tansley's ecosystem as Earth's critical zone. *New Phytol.* **2015**, *206*, 900–912. [CrossRef]
15. Donovan, L.A.; Ehleringer, J.R. Water stress and use of summer precipitation in a Great Basin shrub community. *Funct. Ecol.* **2017**, *8*, 289–297. [CrossRef]
16. Linn, G.H.; Plillips, S.L.; Ehleringer, J.R. Monosoonal precipitation responses of shrubs in a cold desert community on the Colorado Plateau. *Oecologia* **2016**, *106*, 8–17. [CrossRef]
17. Fu, P.L.; Liu, W.J.; Fan, Z.X.; Cao, K.F. Is fog an important water source for woody plants in an Asian tropical karst dry forest during dry season. *Ecohydrology* **2016**, *9*, 964–972. [CrossRef]
18. Cao, J.H.; Yang, H.; Zhang, C.L.; Wu, X.; Bai, B.; Huang, F. Characteristics of structure and material cycling of the karst critical zone in Southwest China. *Geol. Surv. China.* **2018**, *5*, 1–12.
19. Bewley, D.J.; Black, M. *Seeds: Physiology of Development and Germination*; Plenum Press: New York, NY, USA, 2010.
20. Cao, K.F.; Fu, P.L.; Chen, Y.J.; Jiang, Y.J.; Zhu, S.D. Implications of the ecophysiological adaptation of plants on tropical karst habitats for the ecological restoration of desertified rocky lands in southern China. *Sci. Sinica Vitae.* **2014**, *44*, 238–247.
21. Yan, Y.J.; Dai, Q.H.; Hu, G.; Guan, J.; Mei, L.; Fu, W.B. Effects of vegetation type on the microbial characteristics of the fissure soil-plant systems in karst rocky desertification regions of SW China. *Sci. Total Environ.* **2020**, *712*, 136543. [CrossRef]

22. Liu, W.J.; Wang, P.Y.; Li, J.T.; Liu, W.Y.; Li, H.M. Plasticity of source-water acquisition in epiphytic, transitional and terrestrial growth phases of *Ficus tinctoria*. *Ecohydrology* **2014**, *7*, 1524–1533. [CrossRef]
23. Yao, Y.W.; Dai, Q.H.; Gan, Y.X.; Gao, R.X.; Yan, Y.J.; Wang, Y.H. Effects of Rainfall Intensity and Underground Hole (Fracture) Gap on Nutrient Loss in Karst Sloping Farmland. *Sci. Agr. Sin.* **2021**, *54*, 140–151.
24. Guo, Y.L.; Chen, H.Y.; Wang, B.; Xiang, W.S.; Li, D.X.; Li, X.K.; Mallik, A.U.; Ding, T.; Huang, F.Z.; Lu, F.Z.; et al. Conspecific and heterospecific crowding facilitate tree survival in a tropical karst seasonal rainforest. *For. Ecol. Manag.* **2021**, *481*, 118751. [CrossRef]
25. Rempe, D.M.; Dietrich, W.E. Direct observations of rock moisture, a hidden component of the hydrologic cycle. *Proc. Natl. Acad. Sci. USA* **2018**, *115*, 2664–2669. [CrossRef] [PubMed]
26. Wang, J.X.; Zou, B.P.; Liu, Y.; Tang, Y.Q.; Zhang, X.B.; Yang, P. Erosion-creep-collapse mechanism of underground soil loss for the karst rocky desertification in Chenqi village, Puding county, Guizhou, China. *Environ. Earth Sci.* **2014**, *72*, 2751–2764. [CrossRef]
27. Liu, W.J.; Li, P.J.; Duan, W.P.; Liu, W.Y. Dry-season water utilization by trees growing on thin karst soils in a seasonal tropical rainforest of Xishuangbanna, SW China. *Ecohydrology* **2013**, *7*, 927–935. [CrossRef]
28. Luo, X.L.; Wang, S.J.; Bai, X.Y.; Tan, Q.; Ran, C.; Chen, H.; Xi, H.P.; Chen, F.; Cao, Y.; Wu, L.H.; et al. Analysis on the spatio-temporal evolution process of rocky desertification in Southwest Karst area. *Acta Ecol. Sin.* **2021**, *41*, 680–693.
29. Hu, D.; Zeng, F.P.; Song, T.Q.; Liu, K.P.; Wang, K.; Liu, M.X. Water depletion of climax forests over humid karst terrain: Patterns, controlling factors and implications. *Agr. Water Manag.* **2021**, *244*, 3106541.
30. Jiang, Z.C.; Lian, Y.Q.; Qin, X.Q. Rocky desertification in Southwest China: Impacts, causes, and restoration. *Earth Sci. Rev.* **2014**, *132*, 1–12. [CrossRef]
31. Zhong, Y.F.; Hu, X.Y.; Song, X.Q.; Zhou, Z.D. ISSR Analysis on Population Genetic Diversity of *Impatiens hainanensis* (Balsaminaceae), an Endemic Species to Hainan Island. *Chin. J. Trop. Crop.* **2014**, *35*, 1041–1046.
32. Zhong, Y.F.; Wu, H.Z.; Song, X.Q.; Zhou, Z.D. Species Diversity and the Relationship with Habitat Community Characteristics of *Impatiens hainanensis*, Endemic to Hainan Island. *Chin. J. Trop. Crop.* **2014**, *35*, 355–361.
33. Schwinning, S. The ecohydrology of roots in rocks. *Ecohydrology* **2010**, *3*, 238–245. [CrossRef]
34. Wang, M.M.; Chen, H.S.; Fu, T.G.; Zhang, W.; Wang, K.L. Differences of soil nutrients among different vegetation types and their spatial prediction in a small typical karst catchment. *Chin. J. Appl. Ecol.* **2016**, *27*, 1759–1766.
35. Liu, Y.; Han, S.M.; Song, X.Q.; Ding, Q.; Wang, P.; Zhao, Y. Seasonal Variation of Microbial Communities in the Rhizosphere of *Impatiens hainanensis* (Balsaminaceae) at Different Altitudes. *J. Trop. Biol.* **2018**, *9*, 47–53.
36. Craig, H. Isotopic variation in Meteoric waters. *Science* **1961**, *133*, 1702–1703. [CrossRef]
37. Ehleringer, J.R.; Rundel, P.W. *Stable Isotopes in Ecological Research*; Springer: New York, NY, USA, 1988.
38. Chen, Z.S.; Cheng, J.; Guo, P.W.; Lin, Z.Y.; Zhang, F.Y. Distribution Characters and Its Control Factors of Stable Isotope in Precipitation over China. *Trans. Atmos. Sci.* **2010**, *33*, 667–679.
39. Hu, H.Y.; Huang, H.M.; Yang, J.W. Multi time scale variation of hydrogen and oxygen isotopes in precipitation under changing environment in Hong Kong area. *Eng. J. Wuhan Univ.* **2014**, *47*, 577–584.
40. Chen, Y.T.; Du, W.J.; Chen, J.S.; Xu, L.L. Composition of hydrogen and oxygen isotopic of precipitation and source apportionment of water vapor in Xiamen Area. *Acta Sci. Circums.* **2016**, *36*, 667–674.
41. Li, G.; Zhang, X.P.; Xu, Y.P.; Song, S.; Wang, Y.F.; Ji, X.M.; Xiang, J.; Yang, J. Characteristics of Stable Isotopes in Precipitation and Their Moisture Sources in Mengzi Region, Southern Yunnan. *Environ. Sci.* **2016**, *37*, 1313–1320.
42. Song, X.F.; Wang, S.; Xiao, G.Q.; Wang, Z.M. A study of soil water movement combining soil water potential with stable isotopes at two sites of shallow groundwater areas in the North China Plain. *Hydrol. Process.* **2009**, *23*, 1376–1388. [CrossRef]
43. Xu, Q.; Liu, S.; Wan, X.; Jiang, C.Q.; Song, X.F.; Wang, J.X. Effects of rainfall on soil moisture and water movement in a subalpine dark coniferous forest in southwestern China. *Hydrol. Process.* **2012**, *26*, 3800–3809. [CrossRef]
44. Jiang, Y.L.; Bai, K.D.; Guo, Y.L.; Wang, B.; Li, D.X.; Li, X.K.; Liu, Z.S. Floral traits of woody plants and their habitat differentiations in a northern tropical karst forest. *Bio. Sci.* **2016**, *24*, 148–156. [CrossRef]
45. Sun, S.F.; Huang, J.H.; Lin, G.H.; Zhao, W.; Han, X.G. Application of stable isotope technique in the study of plant water use. Ecology. *Acta Ecol. Sin.* **2005**, *25*, 2362–2371.
46. Olmo, M.; Lopez-Iglesias, B.; Villar, R. Drought changes the structure and elemental composition of very fine roots in seedlings of ten woody tree species. Implications for a drier climate. *Plant Soil* **2014**, *384*, 113–129. [CrossRef]
47. Xiong, H.F.; Wang, S.J.; Rong, L.; Cheng, A.Y.; Li, Y.B. Effects of extreme drought on plant species in Karst area of Guizhou Province, Southwest China. *Chin. J. Appl. Ecol.* **2011**, *22*, 1127–1134.
48. Wu, J.E.; Liu, W.J.; Zhu, C.J. Application of Stable Isotope Techniques in the Study of Plant Water Sources and Use Efficiency. *J. Southwest For. Univ. (Nat. Sci.)* **2014**, *34*, 103–110.
49. Gazis, C.; Feng, X. A stable isotope study of soil water: Evidence for mixing and preferential flow paths. *Geoderma* **2004**, *119*, 97–111. [CrossRef]
50. Jia, G.D.; Yu, X.X.; Deng, W.P. Seasonal water use patterns of semi-arid plants in China. *Forest. Chron.* **2013**, *89*, 169–177. [CrossRef]
51. Xu, Q.; Liu, S.R.; An, S.Q.; Jiang, Y.X.; Lin, G.H. Characteristics of Hydrogen Stable Isotope in Soil Water of Sub-Alpine Dark Coniferous Forest in Wolong, Sichuan Province. *Sci. Silvae Sin.* **2007**, *43*, 8–14.
52. Chen, H.S.; Nie, Y.P.; Wang, K.L. Spatio-temporal heterogeneity of water and plant adaptation mechanisms in karst regions: A review. *Acta Ecol. Sin.* **2013**, *33*, 317–326. [CrossRef]

53. Schenk, H.J.; Jackson, R.B. The global biogeography of roots. *Ecol. Monogr.* **2002**, *72*, 311–328. [CrossRef]
54. Liu, W.J.; Li, P.J.; Li, H.M.; Zhang, Y.P.; Duan, W.P. Fog interception and its relation to soil water in the tropical seasonal rain forest of Xishuangbann, Southwest China. *Acta Ecol. Sin.* **2006**, *26*, 9–15. [CrossRef]
55. Yan, Y.J.; Dai, Q.H.; Li, J.; Wang, X.D. Geometric morphology and soil properties of shallow karst fissures in an area of karst rocky desertification in SW China. *Catena* **2019**, *174*, 48–58. [CrossRef]
56. Zhang, Z.F.; You, Y.M.; Huang, Y.Q.; Li, X.K.; Zhang, J.C.; Zhang, D.N.; He, C.X. Effects of drought stress on *Cyclobalanopsis glauca* seedlings under simulating karst environment condition. *Acta Ecol. Sin.* **2012**, *32*, 6318–6325. [CrossRef]
57. Hasselquist, N.J.; Allen, M.F.; Santiago, L.S. Water relationsof evergreen and drought-deciduous trees along a seasonallydry tropical forest chronosequence. *Oecologia* **2010**, *164*, 881–890. [CrossRef] [PubMed]
58. George, L.O.; Bazzaz, F.A. The Herbaceous Layer as a Filter Determining Spatial Pattern in Forest Tree Regeneration. In *The Herbaceous Layer in Forests of Eastern North America*; Oxford University Press: New York, NY, USA, 2003.
59. Zhao, Z.M.; Shen, Y.X.; Zhu, X.A. Research Progress of Soil Moisture in Karst Areas of Southwest China. *Hubei Agr. Sci.* **2017**, *56*, 3603–3609.
60. Tian, L.D.; Yao, T.D.; Sun, W.Z.; Tsujimura, M. Stable isotope in soil water in the middle of Tibetan Plateau. *Acta Pedol. Sin.* **2002**, *39*, 289–295.
61. Jackson, R.B.; Sperry, J.S.; Dawson, T.E. Root water uptake and transport: Using physiological processes in global predictions. *Trends Plant. Sci.* **2000**, *5*, 482–488. [CrossRef]
62. Chen, Y.J.; Cao, K.F.; Schnitzer, S.A.; Fan, Z.X.; Zhang, J.L.; Bongers, F. Water-use advantage for lianas over trees in tropical seasonal forests. *New Phytol.* **2014**, *205*, 128–136. [CrossRef] [PubMed]
63. Deng, X.Q.; Wang, S.J.; Rong, L. Study on Water Sources of Proper Plant Species in Karst Areas. *Earth Environ.* **2012**, *40*, 154–160.
64. Katsanou, K.; Lambrakis, N.; Tayfur, G.; Baba, A. Describing the Karst Evolution by the Exploitation of Hydrologic Time-Series Data. *Water Resour. Manag.* **2015**, *29*, 3131–3147. [CrossRef]
65. Waltham, T. Fengcong, fenglin, cone karst and tower karst. *Carsologica Sin.* **2009**, *28*, 355–369.
66. Brunner, I.; Herzog, C.; Dawes, M.A.; Arend, M.; Sperisen, C. How tree roots respond to drought. *Front. Plant Sci.* **2015**, *6*, 547. [CrossRef] [PubMed]
67. Phillips, R.P.; Ibáñez, I.; D'Orangeville, L.; Hanson, P.J.; Ryan, M.G.; McDwell, N.G. A belowground perspective on the drought sensitivity of forests: Towards improved understanding and simulation. *Forest Ecol. Manag.* **2016**, *380*, 309–320. [CrossRef]
68. Zhou, H.; Zhao, W.Z.; Yang, Q.Y. Root biomass distribution of planted *Haloxylon ammodendron* in a duplex soil in an oasis: Desert boundary area. *Ecol. Res.* **2016**, *31*, 673–681. [CrossRef]
69. Kulmatiski, A.; Beard, K.H. Root niche partitioning among grasses, saplings, and trees measured using a tracer technique. *Oecologia* **2013**, *171*, 25–37. [CrossRef]
70. Xiong, K.; Yin, C.; Ji, H. Soil erosion and chemical weathering in a region with typical karst opography. *Environ. Earth Sci.* **2018**, *77*, 500. [CrossRef]
71. Nie, Y.P.; Chen, H.S.; Wang, K.L. Challenges and probable solutions for using stable isotope techniques to identify plant water sources in karst regions: A review. *Chin. J. Appl. Ecol.* **2017**, *28*, 2361–2368.
72. Xu, Q.; Wang, H.Y.; Liu, S.R. Water use strategies of Malus toringoides and its accompanying plant species *Berberis aemulans*. *Acta Ecol. Sin.* **2005**, *31*, 5702–5710.
73. Kan, H.; Urata, K.; Nagao, M.; Hori, N.; Fujita, K.; Yokoyama, Y.; Nakashima, Y.; Ohashi, T.; Goto, K.; Suzuki, A. Submerged karst landforms observed by multibeam bathymetric survey in Nagura Bay, Ishigaki Island, southwestern Japan. *Geomorphology* **2015**, *229*, 112–124. [CrossRef]
74. Li, H.; Jiang, Z.; Zhou, H.F.; Wang, Y.; Cui, T.S.; Li, Y.; Luo, W.Q. Variation Characteristics of Oxygen and Hydrogen Stable Isotope in Precipitation, Soil Water and Groundwater in the Junggar Basin—Taking Fukang Station of Desert Ecology as a Case. *Res. Soil Water Conserv.* **2008**, *15*, 105–108.
75. Zhu, X.A.; Shen, Y.J.; He, B.B.; Zhao, Z.M. Humus soil as a critical driver of flora conversion on karst rock outcrops. *Sci. Rep.* **2017**, *7*, 12611. [CrossRef] [PubMed]